Journal of Experimental Botany, Vol. 70, No. 8 pp. 2325–2338, 2019
doi:10.1093/jxb/erz023 Advance Access Publication 7 February, 2019

RESEARCH PAPER

Dual and dynamic intracellular localization of *Arabidopsis thaliana* SnRK1.1

Nicolás E. Blanco[1,2,*], Daniela Liebsch[2,3], Manuel Guinea Díaz[4], Åsa Strand[2] and James Whelan[5]

[1] Centro de Estudios Fotosintéticos y Bioquímicos, Universidad Nacional de Rosario (CEFOBI-CONICET/UNR), Rosario, Argentina
[2] Umeå Plant Science Centre, Department of Plant Physiologyogy, Umeå University, Sweden
[3] Instituto de Biología Molecular y Celular de Rosario (IBR-CONICET), Rosario, Argentina
[4] Molecular Plant Biology, Department of Biochemistry, University of Turku, Turku, Finland
[5] Department of Animal, Plant and Soil Science, School of Life Sciences, Australian Research Council Centre of Excellence in Plant Energy Biology, La Trobe University, Bundoora, Victoria 3086, Australia

* Correspondence: blanco@cefobi-conicet.gov.ar

Received 1 October 2018; Editorial decision 8 January 2019; Accepted 1 February 2019

Editor: Christine Raines, University of Essex, UK

Abstract

Sucrose non-fermenting 1 (SNF1)-related protein kinase 1.1 (SnRK1.1; also known as KIN10 or SnRK1α) has been identified as the catalytic subunit of the complex SnRK1, the *Arabidopsis thaliana* homologue of a central integrator of energy and stress signalling in eukaryotes dubbed AMPK/Snf1/SnRK1. A nuclear localization of SnRK1.1 has been previously described and is in line with its function as an integrator of energy and stress signals. Here, using two biological models (*Nicotiana benthamiana* and *Arabidopsis thaliana*), native regulatory sequences, different microscopy techniques, and manipulations of cellular energy status, it was found that SnRK1.1 is localized dynamically between the nucleus and endoplasmic reticulum (ER). This distribution was confirmed at a spatial and temporal level by co-localization studies with two different fluorescent ER markers, one of them being the SnRK1.1 phosphorylation target HMGR. The ER and nuclear localization displayed a dynamic behaviour in response to perturbations of the plastidic electron transport chain. These results suggest that an ER-associated SnRK1.1 fraction might be sensing the cellular energy status, being a point of crosstalk with other ER stress regulatory pathways.

Keywords: Arabidopsis, chloroplast, dual localization, endoplasmic reticulum (ER), ER localization, energy status, *Nicotiana benthamiana*, nuclear localization, retrograde signalling, SnRK1.1.

Introduction

Plant cells harbour two distinct membrane-enclosed endosymbiotic organelles, mitochondria and chloroplasts. Environmental changes are sensed by these organelles, and their functional status is communicated to the nucleus to alter gene expression for a variety of cellular functions through processes known as retrograde signalling pathways (Ng *et al.*, 2014; Chan *et al.*, 2016; Crawford *et al.*, 2018). Both chloroplasts and mitochondria act as environmental sensors due to the direct effect of fluctuating external conditions on the various biochemical functions hosted by them, such as high-light-mediated photoinhibition of PSII function, or cold/salt stress impairment of mitochondrial function. In addition, mitochondria and chloroplasts are both involved in energy production in the cell, operating in opposite ways (consumption and production of reducing equivalents, respectively), which means that these energy organelles have to operate in a co-operative manner under non-limiting as well

as suboptimal growth conditions (Yoshida *et al.*, 2011; Araújo *et al.*, 2014). The direct impact of changes in external conditions on photosynthetic energy production is revealed by the dynamic functioning and composition of the photosynthetic electron transport chain (PETC) and the multiple photoprotective mechanisms that maintain its operative status (Rochaix, 2011; Allahverdiyeva *et al.*, 2015*b*). To establish equilibrium between cellular energy-producing processes, environmental conditions, and optimal growth, plant cells needs to sense the rates of energy production. Although part of the whole regulatory scheme has been studied in recent years (Allahverdiyeva *et al.*, 2015*a*), the mechanisms sustaining this intricate energy homeostasis are far from being understood.

One of the components that has been characterized as an essential part of the plant energy homeostasis system in plants is the SnRK1 [sucrose non-fermenting 1- (SNF1) related protein kinase1] complex. This protein complex has emerged as a central integrator of energy and stress signals, more precisely coordinating the response to conditions that produce a decrease in cellular energy levels (Baena-González and Hanson, 2017). SnRK1 is a plant heterotrimeric kinase complex orthologous to the mammalian AMP-activated protein kinase (AMPK) complex and the SNF1 complex in yeast. It has been proposed that AMPK/SNF1/SnRK1 complexes sense the cellular energy status and maintain energy homeostasis through the control of the balance between anabolic and catabolic metabolism (Hardie *et al.*, 2016). In plants, the α subunit, also known as SnRK1.1, KIN10, or SnRK1α, is the catalytic and main regulatory subunit of the complex (Crozet *et al.*, 2014; Emanuelle *et al.*, 2016). Among the broad set of signalling pathways and developmental processes that are co-ordinated by SnRK1.1, chloroplast and mitochondrial retrograde signalling routes have been proposed as candidates for the source of energy signals to be integrated in this regulatory network (Hartl and Finkemeier, 2012; Ng *et al.*, 2013*a*; Kleine and Leister, 2016).

In the nucleus, the clear role of SnRK1.1 as a regulator of nuclear gene expression has been revealed by the identification of several SnRK1.1-interacting proteins including transcription factors (TFs) (Nietzsche *et al.*, 2014, 2016; Mair *et al.*, 2015; Cho *et al.*, 2016; Nukarinen *et al.*, 2016). The regulation of many developmental and adaptive processes has been assigned to SnRK1.1 (Baena-González and Hanson, 2017), but how and where SnRK1 might be acting as a sensor of the cellular energy status remains unclear (Emanuelle *et al.*, 2016). A second intracellular position of SnRK1.1 outside the nucleus has also been widely reported, but the exact nature and significance of this non-nuclear localization is yet to be defined. Fluorescence puncta have been frequently visualized when fluorescent-tagged SnRK1.1 is expressed in *Nicotiana benthamiana* and Arabidopsis (López-Paz *et al.*, 2009; Bitrián *et al.*, 2011; Tsai and Gazzarrini, 2012; Williams *et al.*, 2014; O'Brien *et al.*, 2015). Recently, experiments on co-localization with FCS-like zinc finger proteins suggested a non-nuclear localization of SnRK1.1 associated with the endoplasmic reticulum (ER) of onion epidermal cells (Jamsheer *et al.*, 2018*a*, b). However, apart from these reports, most of the research has been focused on understanding the function of the nuclear SnRK1.1 fraction. The relationship of the localization/function of the non-nuclear subpopulation has not been studied in detail, and how this kinase is able to regulate such a number and diversity of processes remains uncharacterized (Emanuelle *et al.*, 2016).

This work presents the results of a thorough investigation of the localization of SnRK1.1 in plant cells using two different biological systems under physiological conditions (*N. benthamiana* and Arabidopsis), different imaging techniques (epifluorescence microscopy combined with a structured light illumination device, spinning disc, and laser scanning confocal microscopy), and spatio-temporal co-localization studies with intracellular markers. In addition, we evaluated the effect of perturbations of the chloroplasts on SnRK1.1 distribution. These studies showed that under physiological conditions, SnRK1.1 is partitioned between the nucleus and a non-nuclear fraction associated with the ER. When the plants were treated with inhibitors to perturb plastid energy production, this dual distribution was affected, supporting a role for SnRK1.1 as a sensor of cellular energy status integrating signals from chloroplasts.

Materials and methods

Vector construction and Agrobacterium *strains*

Using genomic DNA as template, the regulatory and the coding sequence of SnRK1.1 was amplified starting at position −739 from the initial ATG belonging to splicing form At3g01090.1 of SnRK1.1. The resulting fragment covers the whole intergenic region before the upstream gene (*HYP1*, At3G01100), and allows the formation of a C-terminal fusion with the enhanced green fluorescent protein (eGFP) coding sequence of pSITE2NB (Chakrabarty *et al.*, 2007). The primers used to clone this genomic fragment into pDONR207 are SnRK1.1 Fw 5' GGGGACAAGTTTGTACAAAAAAGCAGGCT ATGATGACTAGATGCCACGTCC and SnRK1.1 Rv 5' GGGGACCACTTTGTACAAGAAAGCTGGGT GGAGGACTCGGAGCTGAGCAAG (with the attB flanking region underlined in the primer sequences). Two consecutive reactions using BP clonase and LR clonase Gateway© (Invitrogen) generated the final vector containing SnRK1.1–GFP. *Agrobacterium tumefaciens* [GV3101(pMP90)] was transformed with this plasmid, an ER marker fused to mCherry (ER-rb) (Nelson *et al.*, 2007), and nuclear-targeted histone 2b fused to the red fluorescent protein tag of the pSITE-4CA binary vector (H2b–RFP) (kindly provided by Edoard Pesquet). The ER marker (ER-rb) is a chimeric protein containing the signal peptide of *At*WAK2 (*Arabidopsis thaliana* wall-associated kinase 2) at the N-terminus of the RFP and the ER retention signal His-Asp-Glu-Leu at its C-terminus. The fusion protein is encoded on a vector containing resistance to BASTA for selection in plants (Nelson *et al.*, 2007). All *Agrobacterium* strains were grown on YEB plates using selection antibiotics rifampicin (50 μg ml^{-1}), gentamycin (20 μg ml^{-1}), and spectinomycin (100 μg ml^{-1}) or kanamycin (50 μg ml^{-1}). Colonies were grown for 48 h in a 28 °C chamber and used for infiltration of *N. benthamiana* leaves or stable transformation of Arabidopsis by floral dip and sexual crosses.

Plant growth conditions

Nicotiana benthamiana plants were grown for 4–8 weeks in a growth chamber under a 16 h 180 μmol photon m^{-2} s^{-1}/8 h dark regime with temperatures of 23 °C/21 °C. Arabidopsis lines were selected on half-strength Murashige and Skoog (1/2 MS) supplemented with 35 μg ml^{-1} kanamycin for initial selection of SnRK1.1–GFP transgenic lines, and a further 5 μg ml^{-1} Basta for the selection of mutants expressing ER-rb. Twelve-day-old plants were transferred to soil to complete the life cycle.

Agrobacterium *infiltration of* N. benthamiana *leaves*

Agrobacterium infiltration was carried out into young leaves (4–8 weeks) of *N. benthamiana* based on previously described protocols (Sparkes *et al.*, 2006; de Felippes and Weigel 2010), with the following modifications: each strain carrying an organelle fluorescence marker and/or

SnRK1.1–GFP-expressing vector was diluted in freshly prepared infiltration medium (10 mM MES pH 5.8, 10 mM $MgCl_2$, and 150 μM acetosyringone) to OD_{600}=0.3–0.5. *Agrobacterium* suspensions were incubated in darkness for at least 3 h. During this incubation time, *N. benthamiana* plants were well watered to favour the spreading of the infiltration mix across the leaves. After incubation, leaves were infiltrated at only one position of the leaf on the abaxial side, and only leaves that had internalized *Agrobacterium* suspension across the whole leaf surface were further evaluated. Sections were collected maximally after 48 h post-infiltration from the opposite blade side to the infiltration point of healthy leaves to avoid any mechanical stress artefacts.

Cell energy perturbation treatments

To conduct cell energy perturbation experiments, we selected infiltrated plants growing in chambers for maximally 48 h after infiltration in the case of the preliminary studies in *N. benthamiana*. Similar canopy fully expanded adult leaves were sprayed with control solution (water or a dilution of DMSO) and 50 μM DCMU [3-(3,4-dichlorophenyl)-1,1-dimethylurea] or 100 μM DBMIB (2,5-dibromo-3-methyl-6-isopropyl-*p*-benzoquinone) (to perturb electron transfer reactions in chloroplasts) before imaging. In the case of DBMIB, spraying treatments were repeated hourly to overcome instability of the compounds (Blanco *et al.*, 2014). Stability of DCMU was previously evaluated and only one treatment was conducted per experiment (Kindgren *et al.*, 2012). Final observations were conducted in transgenic Arabidopsis lines expressing ER-rb and SnRK1.1–GFP.

Fluorescence microscopy imaging

Sections of corresponding infiltrated leaves were analysed by epifluorescence microscopy with the AxioImager.Z2 with APOTOME2 system based on structured illumination, and laser scanning confocal microscopy (LSCM) using the system Zeiss LSM 780 and 880 Axio Observer with an upright microscope stand. For imaging, in the first case an Objective Plan-Apochromat ×63/1.40 oil DIC M27 was used and the LSM 880 was configured with a Plan-Apochromat ×20/0.8 M27, also used for DIC (differential interference contrast) during bright field acquisition. For GFP detection with the Zeiss LSM 880, a 488 nm excitation laser line was used and the emission was collected between at 490 nm and 526 nm. For mCherry/RFP detection, the imaging settings were excitation at 543 nm and emission detection in the range of 575–606 nm. Finally, autofluorescence of chlorophyll was indirectly observed in the GFP channel during the epifluorescence microscopy imaging. For LSCM imaging, the excitation was conducted at 543 nm and the emission was collected 690–710 nm. The images with Axio Imager.Z2 were obtained by excitation with a metal-halide lamp HXP 120 C and Filter Cubes for GFP (38 GFP BP EX 470/40 nm BS FT 495 EM BP 525/50 nm) and mCherry/RFP (63 HE BP EX 572/25 nm BS FT 590 EM 629/62 nm) using an Axiocam 506.

Regarding the specimens used for imaging, in all cases more than three independent transformation experiments were used for imaging control conditions in the *N. benthamiana* system. Images were obtained from sections of independent leaves, either infiltrated or belonging to Arabidopsis stable lines. Several independent stable lines were initially evaluated, and detailed imaging was performed for three stable lines. Initial imaging of the DCMU and DBMIB treatments was done on the Arabidopsis lines expressing only SnRK1.1–GFP, and at least two independent experimental repetitions were conducted in Arabidopsis lines expressing both SnRK1.1–GFP and the ER marker, exhibiting the same pattern.

Subcellular fractionation and western blotting of total, soluble, and microsomal fractions

Nicotiana benthamiana infiltrated leaves and Arabidopsis transgenic lines together with mock-infiltrated and control Arabidopsis lines were used to separate soluble protein and the microsomal fraction. The protocol was adapted from Kriechbaumer (2016) and(Cecchini *et al.* (2015). Briefly, 2 g of leaves were ground in liquid nitrogen and homogenized in 4 ml of buffer A (50 mM Tris–HCl, pH 7.5; 0.33 M sucrose; 5 mM EDTA; 150 mM NaCl, and 1× complete protease inhibitor cocktail from Roche). The total protein extract was obtained by filtering the crude extract through two layers of Miracloth and centrifuged at 10 000 *g* for 10 min. Afterwards a second centrifugation at 93 000 *g* for 90 min (swing-out rotor; SW41), with a cushion of buffer A with 0.5 M sucrose, was conducted to obtain the cytosolic fraction (supernatant). The pellet was resuspended in 250 μl of buffer A, leading to the microsomal fraction. Total, microsomal, and cytosolic fractions were separated on a 10% (v/v) SDS–polyacrylamide gel, transferred to a polyvinylidene difluoride (PVDF) membrane, and probed with anti-GFP -specific antibodies (1:400) and anti-SnRK1.1 antibodies (1:500, Agrisera) for all fractions. The membrane was further incubated with anti-rabbit immunoglobulin G conjugated with horseradish peroxidase (HRP) and the signal was detected with A ChemiDoc (Touch) Biorad Scanner using Chemiluminescence mode with Super Sigal West femto (Thermo Scientific).

Results

SnRK1.1 localization prediction

Previous *in vivo* localization studies have not unequivocally identified the intracellular localization of SnRK1.1. Supplementary Table S1 at *JXB* online summarizes *in vivo* studies that have been conducted directly or indirectly to establish the localization of SnRK1.1. A clear localization in the nucleus is accepted by all the studies, but the presence of SnRK1.1 in a second location remains inconclusive. The non-nuclear fraction of SnRK1.1 has been found in the cytoplasm and/or in fluorescent structures such as puncta. One critical aspect in previous studies has been the choice of the SnRK1.1 splicing forms used for the analysis. Public databases contain three different spliced forms (At3g01090.1, 2, and 3) with 10 common exons, and a differential exon at the N-terminal end. Based on RNA sequencing (RNAseq) data of a study centred on alternative splicing processes under light conditions in leaves (Mancini *et al.*, 2016), At3g01090.1 is the form most highly expressed in illuminated leaves and was selected to predict localization (Supplementary Fig. S1A). Using the Bio-Analytic Resources for Plant Biology platform, we evaluated SnRK1.1 through SUBA4, a database that houses information on protein interaction and localization based on bioinformatics predictions (Hooper *et al.*, 2017). The results, displayed in an electronic fluorescent pictograph, indicate the cytosol, mitochondrion, and nucleus as possible intracellular locations for SnRK1.1 (Supplementary Fig. S1B) (Winter *et al.*, 2007). A subsequent analysis by using individual algorithms led to similar results. AdaBoost, EpiLoc, MultiLoc2, WoLF PSORT, and YLoc predicted a cytosolic localization; SubLoc, PProwler, and SLPFA reported protein targeting to mitochondria; and BaCelLo, Plant-mPloc, and SLP-Local indicated a nuclear localization, the latter also predicting a cytosolic distribution. Furthermore, only the recently published LOCALISER 1.0.2 (Sperschneider *et al.*, 2017) predicted one nuclear localization signal (Supplementary Fig. S1C). This software has been specially designed to detect targeting sequences to mitochondria and plastids, in plant proteins and pathogen effector proteins. The lack of detection of a targeting sequence with this computational prediction method, together with the other inconclusive results of bioinformatics, provides evidence against the presence of any targeting sequence in SnRK1.1. The absence of a clear bioinformatics prediction led us to

perform a detailed localization study *in planta* using the model system of *N. benthamiana* and *Arabidopsis thaliana*.

SnRK1.1 co-localizes with nuclear and ER markers in the N. benthamiana *transient expression system*

To determine the *in planta* localization of SnRK1.1, the entire genomic sequence of SnRK1.1 including the native promoter and 5'-untranslated region (UTR) were cloned in frame to the N-terminus of eGFP in vectors of the pSITE series (Chakrabarty *et al.*, 2007) and used to infiltrate young and healthy leaves of *N. benthamiana*. This cloning strategy covers the expression of any alternative splicing variants by using eGFP fused to the common C-terminal domain of the three different variants. Initially, imaging was performed using epifluorescence microscopy (EF) with the aim of capturing higher amounts of fluorescence signal compared with LSCM. The APOTOME system allowed optical sectioning using structured illumination (SIM) (Weigel *et al.*, 2009). The images obtained of *N. benthamiana* leaves, co-infiltrated with SnRK1.1–GFP and a nuclear fluorescent marker (H2b–RFP), are presented in Fig. 1. Confirming previously reported results, SnRK1.1–GFP was observed in the nucleus, co-localizing with H2b–RFP (Fig. 1A–J). Although both fluorescent-tagged proteins were found to co-localize at the nucleus position, SnRK1.1–GFP and H2b–RFP did not exhibit the exact same signal pattern (Fig. 1A–E, F–J). These differences were also visualized in images obtained along the *z*-axis (Supplementary Fig. S2A, B). The imaging along the *z*-axis provided spatial information that confirmed the presence of SnRK1.1 both inside and outside the nucleus, taking as reference for the nuclear compartment the H2b–RFP distribution. Interestingly, the pattern of SnRK1.1 fluorescence signal was frequently observed in ring-like structures surrounding the H2b–RFP signal, possibly delineating the nuclear envelope, and as discrete structures inside the nucleus. These fluorescent nuclear bodies were previously identified as subnuclear foci, positions where SnRK1.1 interacts with DUF581 proteins, and which show similarities with nuclear bodies or speckles in animals (Mao *et al.*, 2011; Nietzsche *et al.*, 2014).

As well as the nucleus-associated fraction, a second fraction of SnRK1.1–GFP was distributed in a non-nuclear intracellular location [Fig. 1A–E, dotted-line region of interest (ROI); magnified in Fig. 1K–O]. Here, the SnRK1.1–GFP signal exhibited a pattern of tubules and discrete sheets in a network-like structure, in some parts closely associated with or surrounding the position of chloroplasts. This pattern of SnRK1.1–GFP was also observed using LSCM in *N. benthamiana* (Supplementary Fig. S3) and in primary Arabidopsis transformants expressing SnRK1.1–GFP (Supplementary Fig. S4) in pavement cells of adult leaves and also in the vascular tissue, an area that has high levels of expression of SnRK1.1 (Williams *et al.*, 2014).

Specific features of this non-nuclear SnRK1.1–GFP signal pattern observed in both stable Arabidopsis lines and transient

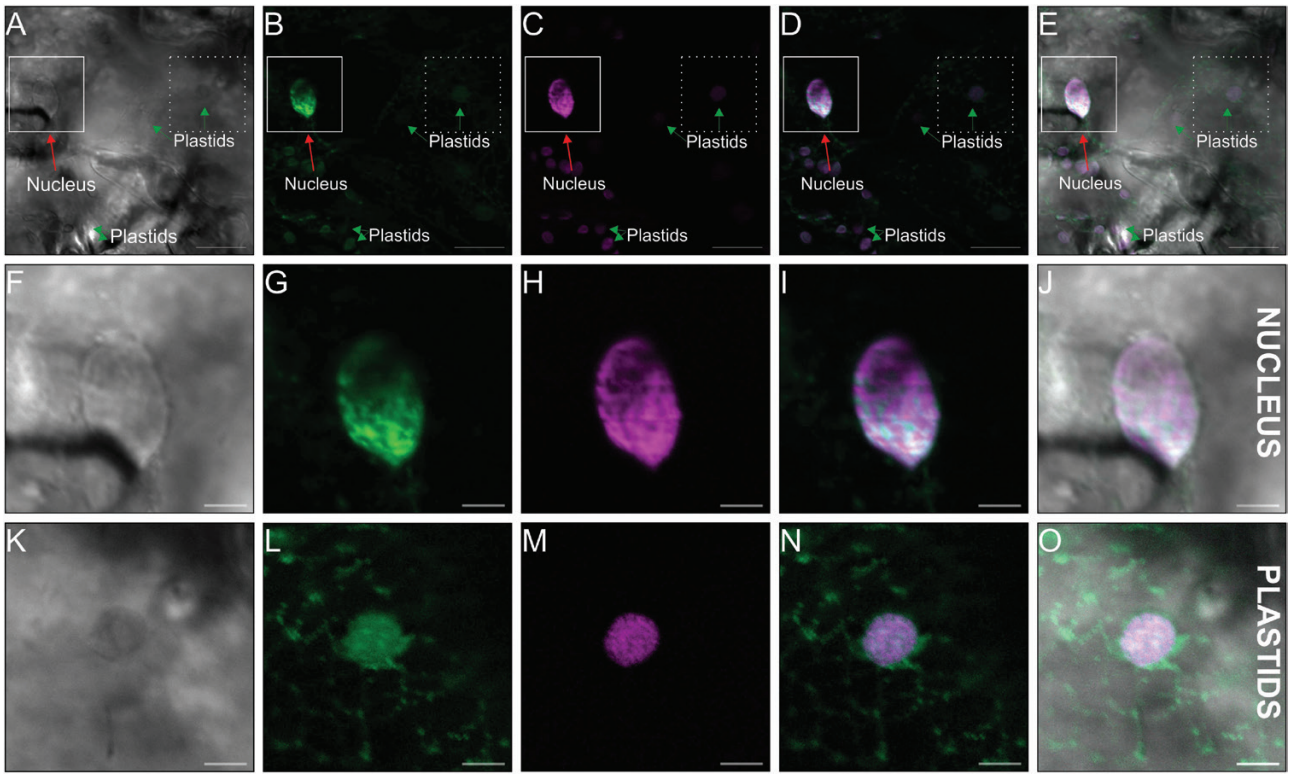

Fig. 1. Nuclear localization of SnRK1.1 in epidermal *N. benthamiana* cells. Images obtained by EF-SIM of leaves transiently expressing SnRK1.1–GFP and H2b–RFP. (A–E) Images of DIC, green channel (SnRK1.1–GFP), red channel (H2b–RFP), the merged signal of fluorescence channels, and all channels merged, respectively. Red arrows indicate the position of the nucleus and green arrows show the position of the plastid. Two regions of interests (ROIs) are centred at the position of the nucleus (continuous-line square, ROI 1) and on the network-like structure confining chloroplasts (dotted-line square, ROI 2). (F–J and K–O) Zoomed-in images of ROI 1 and 2, with the same distribution of channels and merged images as in (A–E). Scale bars: 20 μm (A–E), 5 μm (K–O).

N. benthamiana infiltrated leaves have similarities to ER morphology. ER morphology in leaves has been described as network shaped in tubular and planar sheet structures, in some cases around chloroplasts (Stefano *et al.*, 2014; Hawes *et al.*, 2015). To reveal the identity of the non-nuclear SnRK1.1 structures, co-localization experiments were conducted using an ER marker, hereinafter referred to as ER-rb [ER marker fused to mCherry red fluorescent protein selectable for BASTA resistance, as it is named in the original work (Nelson *et al.*, 2007); details of the construct are given in the Materials and methods]. The overlap between ER-rb and SnRK1.1–GFP signals was observed both by LSCM and EF-SIM in *N. benthamiana*-co-infiltrated leaves when imaging was performed along the *z*-axis perpendicular to the leaf surface (Fig. 2 and Supplementary Fig. S5, respectively). By imaging a *z*-stack series using both types of fluorescence microscopy, we observed tubules and sheet structures at the cortical level (magenta ovals in Fig. 2) and structures surrounding chloroplasts (red ovals in Fig. 2). In addition, the SnRK1.1 signal also overlaps with the ER perinuclear ring, a distinctive hallmark of the spatial ER morphology (Fig. 2N–P) (Sparkes *et al.*, 2009*a*). Altogether, this evidence suggests that SnRK1.1 co-localizes with both nuclear- and ER-targeted fluorescence markers.

The analysis of the SnRK1.1 distribution across the whole cell in 3D reconstructions rendered using *z*-stack (Supplementary Video S1) showed that the co-localization of SnRK1.1 with ER-rb was clear in the ER structures composed of long strands and in the perinuclear zone. The overlap in cortical zones was less pronounced (i.e. in the tubules of the cortical ER) (Fig. 2; Supplementary Fig. S5; Supplementary Video S1; Supplementary Table S2). Higher co-localization values were observed in ER zones close to the nucleus than in cortical zones (tM2 values indicate the co-localization of SnRK1.1–GFP signal when ER-rb signal is above a threshold). In all cases the 'thresholding' method was according to Costes' approach and *P*-values=1 indicated the highest degree of significance in the co-localization values (Bolte and Cordelières, 2006). To evaluate if this uneven SnRK1.1 distribution among the different ER domains was a consequence of the dynamic feature of the non-nuclear fraction of SnRK1.1, experiments of imaging in time were conducted using spinning disc confocal microscopy and a second set of fluorescent markers. Imaging was conducted in *N. benthamiana* leaves co-expressing 3-hydroxy-3-methylglutaryl CoA reductase (HMGR) fused to GFP (Leivar *et al.*, 2005; Ferrero *et al.*, 2015), as a marker of the ER, and SnRK1.1 fused to RFP (Chakrabarty *et al.*, 2007). HMGR has been previously reported as a target protein of the kinase activity of SnRK1.1 (Rodríguez-Concepcion and Boronat, 2015). Using the same approach as before, a series of images were obtained along the *z*-axis with focal planes localized at the cortical zone of epidermal cells of co-infiltrated *N. benthamiana* leaves (Fig. 3). The obtained images indicated that SnRK1.1–RFP and HMGR–GFP co-localize at the cortical zone of epidermal cells. The stability of co-localization between HMGR and SnRK1.1 was further evaluated by imaging a selected plane in a time course for 30 s (Supplementary Fig. S6). The whole time series of images is presented in Supplementary Video S2. These sets of images show that SnRK1.1 co-localization with proteins targeted to the ER is stable over a time frame of minutes and also exhibits a dynamic similar to ER structures.

In summary, the results obtained through the usage of three alternative microscopy approaches and two different sets of fluorescence markers showed that SnRK1.1 is present in the nucleus and also co-localizes with ER-targeted proteins in the *N. benthamiana* system.

Dual localization of SnRK1.1 in stable transgenic Arabidopsis lines

After the set of SnRK1.1 co-localization experiments in *N. benthamiana* including nuclear and ER markers, we evaluated whether the original signal pattern observed in transgenic Arabidopsis lines expressing SnRK1.1 also displayed co-localization with the ER. For this purpose, we generated transgenic stable lines co-expressing SnRK1.1–GFP and ER-rb (Nelson *et al.*, 2007). As in the transient system, SnRK1.1–GFP and ER-rb exhibited a similar intracellular distribution (Fig. 4). Serial imaging along the *z*-axis showed the presence of SnRK1.1–GFP in laminar and tubular structures co-localizing with ER-rb (magenta ovals, Fig. 4A–D). SnRK1.1 was also found in the nucleus of Arabidopsis transgenic lines (white squares, Fig. 4E–Q). A 3D reconstruction of intracellular SnRK1.1 and ER-rb distribution in transgenic Arabidopsis lines using the fluorescent channel images of a *z*-stack covering ~9.13 nm of depth is shown in Supplementary Fig. S7 and Supplementary Video S3. During the original screening, in addition to the pavement cells of leaves of Arabidopsis, vascular tissue also exhibited detectable expression of SnRK1.1–GFP signal driven by the endogenous promoter (Williams *et al.*, 2014). When this tissue was imaged in the stable Arabidopsis lines expressing both markers, a similar co-localization of SnRK1.1–GFP and ER-rb signals was observed (Supplementary Fig. S7).

The results of the studies on co-localization in leaves of stable *A. thaliana* transgenic lines confirmed the previous analysis in *N. benthamiana*. They demonstrate that the partitioning of *A. thaliana* SnRK1.1 between the ER and nucleus occurs in its native context (i.e. the Arabidopsis regulatory context) and at physiological levels (use of a native promoter to drive the expression of the fusion protein) for tissues with photosynthetic activity. These observations exclude side effects intrinsic to the heterologous expression system, such as mechanical wounding or artefacts linked to overexpression of alien proteins (O'Brien *et al.*, 2015).

SnRK1.1–GFP is detected in microsomal and soluble fractions

In order to obtain complementary evidence of the association of SnRK1.1–GFP with the ER, we isolated different intracellular fractions from leaf tissue expressing this fusion protein followed by immunodetection. Total, soluble, and microsomal fractions of infiltrated *N. benthamiana* leaves transiently expressing SnRK1.1–GFP and stable Arabidopsis lines transformed with the same construct were studied using antibodies against SnRK1.1 and GFP. For total protein extracts,

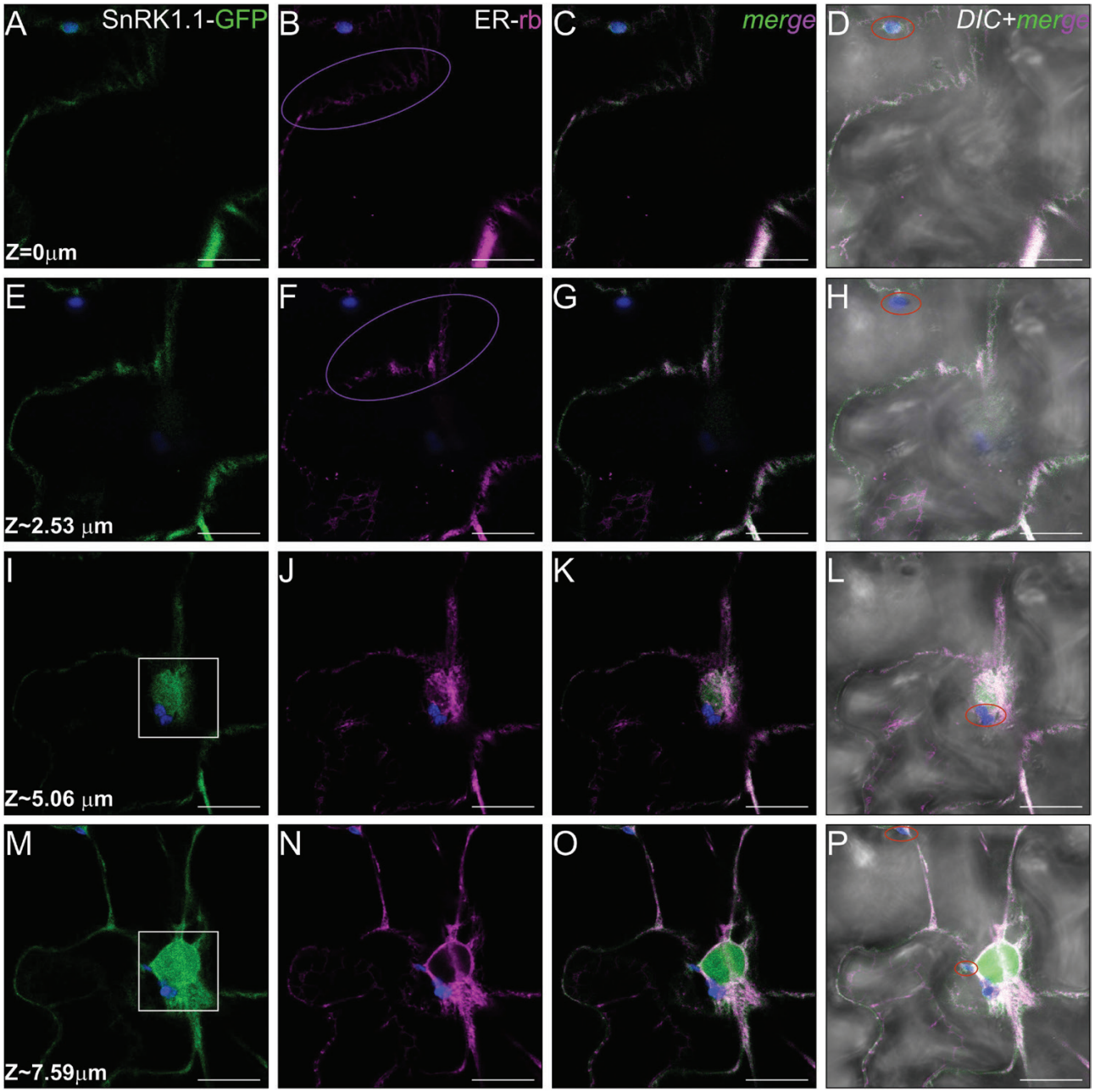

Fig. 2. ER localization of SnRK1.1 in epidermal *N. benthamiana* cells. SnRK1.1 and the ER-marker (ER-rb) expressed transiently in *N. benthamiana*. Images obtained by LSCM of *N. benthamiana* leaf sections simultaneously expressing SnRK1.1–GFP (green channel) and ER-rb (red channel). The type of fluorescence signal or the merging conditions used are indicated at the top of the columns. All fluorescent channels include chlorophyll autofluorescence signal (blue). Each vertical set of images belongs to a specific consecutive optical plane separated by ~2.53 nm and obtained transversally to the *z*-axis. The upper set of images were obtained from the adaxial plane in the zone of the cortical ER (A–D) (marked with magenta ovals), and the following sets include the ER perinuclear ring and strands from the upper to the lower nuclear position, with (M–P) being the the most internal section of the *z*-stack. The position of the nucleus (white continuous line square, I and M) was determined by the position of the ER perinuclear ring structure. Red ovals show chloroplasts surrounded by ER structures. Scale bars: 20 μm.

two different bands were observed in infiltrated *N. benthamiana* leaves with SnRK1.1–GFP for both antibodies (Fig. 5A; Supplementary Fig. S8A), of which one corresponds to the expected size of the fusion protein (~90 kDa, filled arrow). The identity of the second band cannot be determined (>100 kDa, open arrow), though it seems not to be unspecific background, as it was not observed in mock-transformed plants. In extracts from Arabidopsis, besides unspecific bands also observed in the wild type, a similar pattern was obtained in the total extract from Arabidopsis transgenic stable lines (Fig. 5B; Supplementary Fig. S8B). Total protein extract was further separated into a fraction containing ER-enriched microsomes and a soluble part containing other organelles including nuclei by ultracentrifugation based on the protocols of Cecchini *et al.* (2015) and Kriechbaumer *et al.* (2015). The identity of the microsomal fraction was confirmed using antibodies against binding immunoglobulin protein (BiP) (Supplementary Fig. S8C). From the comparison of the signal pattern obtained for

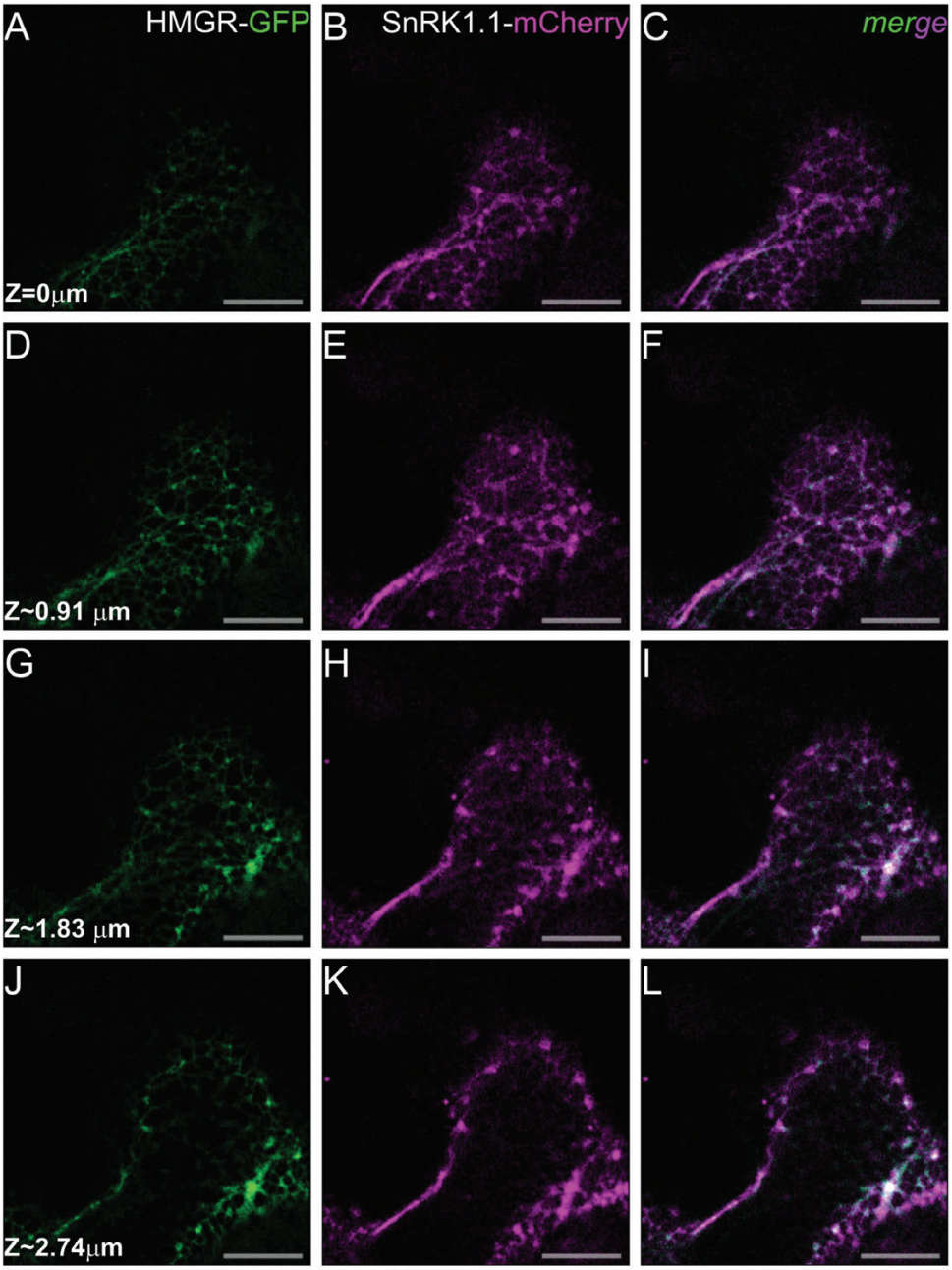

Fig. 3. Co-localization of SnRK1.1 with the ER resident protein 3-hydroxy-3-methylglutaryl coenzyme A reductase (HMGR). Images were obtained by fluorescence microscopy using a spinning disc unit device at the cortical area of epidermal cells of *N. benthamiana* expressing HMGR–eGFP and SnRK1.1–mCherry. Panels show images corresponding to individual and merged channels along the *z*-axis, with optical planes separated by ~0.91 nm. Scale bars: 10 μm.

soluble and microsomal fractions for both *N. benthamiana* and Arabidopsis, we could indeed detect a signal in the microsomal fraction, which would support that SNRK1 is associated with the ER. Additionally, we observed a differential distribution of the different SnRK1.1 forms in each subcellular preparation. In Arabidopsis protein extracts, only one discrete band was detected by western blot in microsomal fractions, consistent with the expected molecular weight (filled arrow, Fig. 5B).

The finding of different electrophoretic mobility forms detected by either anti-SnRK1.1 or anti-GFP antibodies revealed the existence of different post-translational modifications of electrophoretic mobility of SnRK1.1–GFP. These modifications have been proposed to affect kinase activity, stability, and subcellular localization (Crozet *et al.*, 2014). The unique signal observed in the microsomal fraction might be indicative of a specific function depending on a particular modification associated with ER membranes. For the β subunits 1 and 2 (SnRKβ1 and 2), a correlation between post-translational modification (myristoylation) and intracellular distribution has been demonstrated (Pierre *et al.*, 2007).

Changes in SnRK1.1–GFP intracellular distribution by perturbation of the cellular energy status

Our findings showed that the non-nuclear fraction of SnRK1.1 is associated with the ER, and that it co-localizes with potential target proteins at the ER within short time periods,

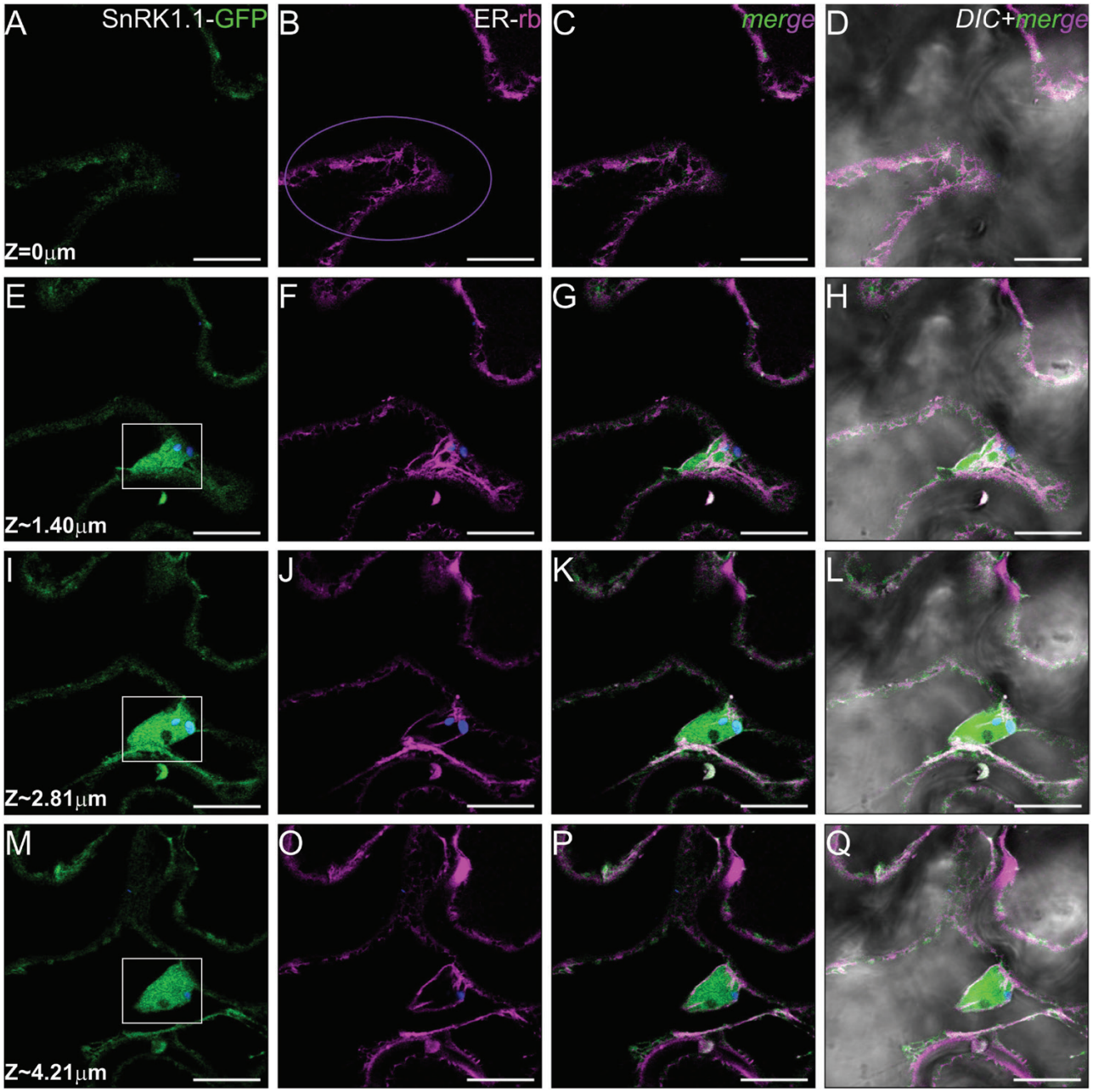

Fig. 4. SnRK1.1 and the ER marker (ER-rb) expressed in stable transgenic Arabidopsis lines. Images obtained by LSCM of Arabidopsis stable transgenic lines simultaneously expressing SnRK1.1–GFP (green channel) and ER-rb (red channel). The type of fluorescence signal or the merging conditions used are indicated at the top of the columns. All fluorescent channels include chlorophyll autofluorescence signal (blue). Each vertical set of images belongs to a specific consecutive optical plane separated by ~1.40 nm and obtained transversally to the *z*-axis. The upper set of images were obtained from the most adaxial plane in the zone of cortical ER (A–D) (marked with a magenta oval), and the following sets include the ER perinuclear ring and strands from the upper to the lower nuclear position, with (M–Q) being the most internal section of the *z*-stack. The position of the nucleus (white continuous line square, E, I, and M) was determined by the position of the ER perinuclear ring. Scale bars: 20 μm.

thus exhibiting a dynamic behaviour (Supplementary Fig. S6; Supplementary Video S2). This supports that ER association of SnRK1.1 is of functional significance and, in turn, considering the presence of two fractions (nuclear and non-nuclear) puts forward the idea of a dynamic behaviour to connect both intracellular compartments.To explore whether SnRK1.1 has a dynamic behaviour that might be involved in its proposed role as an energy sensor (Baena-González and Hanson, 2017), we analysed the spatial SnRK1.1 distribution in response to the chloroplast redox status.Treatments with DCMU and DBMIB were employed to perturb the cellular energy status directly by selective inhibition of the PETC in chloroplasts. DCMU treatments had originally been used to trigger the SnRK1.1-mediated low-energy response by blocking the plastoquinone-binding site of PSII (Baena-González *et al.*, 2007). In the case of DBMIB, the imposed imbalance at the PETC is similar to conditions of excess energy, suich as, for instance, high-intensity illumination (Blanco *et al.*, 2014). The treatments were conducted during 2 h and 3 h, respectively, in leaves of Arabidopsis lines expressing SnRK1.1–GFP and ER-rb with

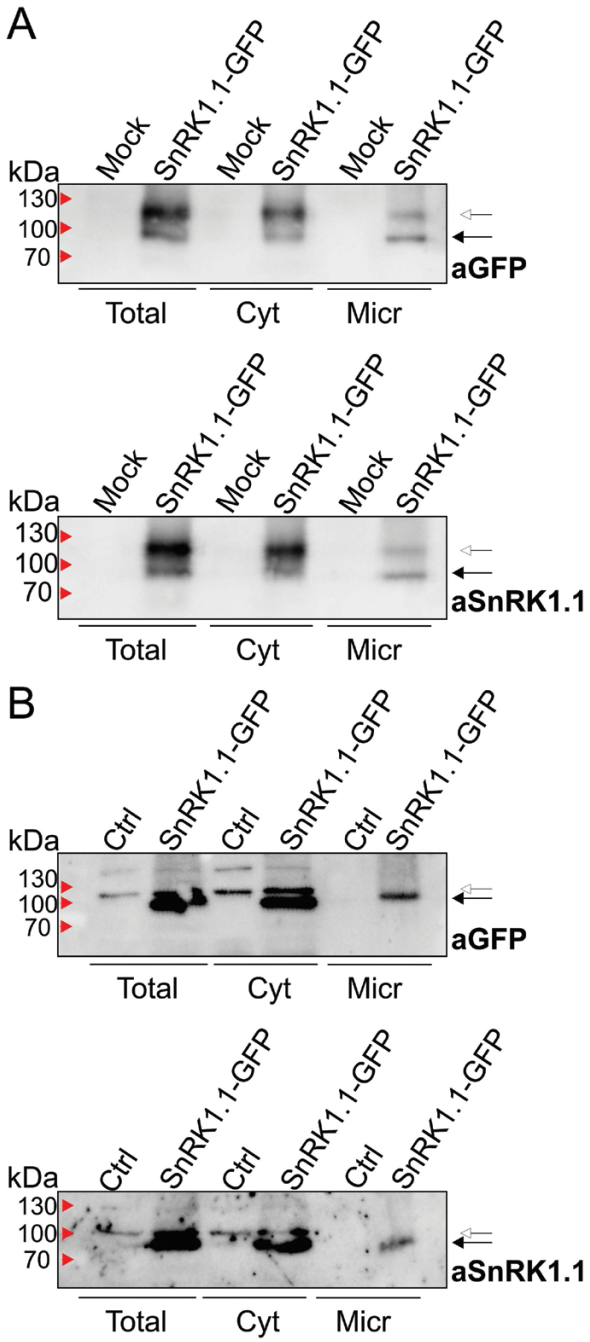

Fig. 5. Immunoblot analysis of subcellular fractions of infiltrated *N. benthamiana* leaves (A) and Arabidopsis stable transgenic lines expressing SnRK1.1 (B). Total, cytosolic (Cyt), and microsomal (Micr) fractions of *N. benthamiana* leaves and Arabidopsis transgenic lines expressing SnRK1.1–GFP proteins were immunoanalysed to detect this transgenic protein using different antibodies. Antibodies against GFP (upper panels in A and B) and SnRK1.1 (lower panels) were used to detect the SnRK1.1–GFP protein against the same extract. Black arrows at the right side of the corners indicate immunoreactive signals of the expected molecular weight, and empty arrows indicate extra electrophoretic forms. (This figure is available in colour at *JXB* online.)

inhibitor concentrations that provoked a complete blockage of the PETC as previously reported in studies of plastidic retrograde signals (Blanco *et al.*, 2014).

The effect of treatments on intracellular SnRK1.1 distribution was visualized by the use of maximum intensity projection on images obtained along the *z*-axis (covering ~5 μm) of transgenic Arabidopsis leaves expressing SnRK1.1 and ER-rb (Fig. 6A–C, E–G, I–K) and by 3D reconstruction based on these sets of images (Fig. 6D, H, L). The over-reduction of the plastoquinone pool mediated by DBMIB provoked the appearance of SnRK1.1–GFP aggregates concomitantly with the loss of the SnRK1.1–GFP signal localized to tubule-shaped structures (Fig. 6E, G, H). In addition to these changes, ER morphology was also affected by DBMIB treatment, with a lower proportion of tubules compared with small sheet-like structures (Fig. 6F, also observed in the images merged with SnRK1.1–GFP signal). On the other hand, DCMU treatment affected the SnRK1.1 and ER-rb distribution to a lesser degree than the DBMIB treatment. SnRK1.1 non-nuclear signal was more diffuse than in control conditions, as visible both in the maximum intensity projection images and in the 3D reconstruction (Fig. 6I–L in comparison with A–D). The DCMU results do not show an SnRK1.1-mediated low-energy response through an intracellular change in its distribution in epidermal cells. To address the reasons for this situation, we evaluated the distribution of SnRK1.1 in vascular tissue of the same Arabidopsis transgenic lines. Under the same treatment conditions, we detected a profound change in the distribution of SnRK1.1, with an increase of the signal of the nuclear SnRK1.1 fraction compared with the non-nuclear signal (Fig. 7). The treatment also affected the ER status, by the appearance of a discrete number of ER bodies, which are revealed by an intense accumulation of ER-rb signal in cigar-shaped forms (Fig. 7E, F).

In summary, the DCMU and DBMIB treatments revealed the sensitivity of the intracellular SnRK1.1 distribution to changes in cellular energy status caused by imbalances at the PETC. These observations reinforce the idea of the ER as a connecting network integrating information about other organelles, such as, for instance, the chloroplast energy status.

Discussion

SnRK1 is one of the most studied kinase complexes in plants due to the wide range of metabolic reactions and physiological processes that are linked to it. The heterotrimeric SnRK1 complex has been directly identified as a key player in responses regulated by energy status, though the underlying mechanisms are not fully understood (Broeckx *et al.*, 2016; Baena-González and Hanson, 2017). The function, activity, and regulation of its catalytic subunit SnRK1.1 (also known as AKIN10 or SnRK1α) have been addressed in several studies with the aim of gaining insight into the mechanisms that contribute to maintaining cellular energy homeostasis. Most of the evidence has been obtained by linking the function of a TF directly related to a developmental process with the nuclear fraction of SnRK1.1 (reviewed in Baena-González and Hanson, 2017). In almost all cases, the presented intracellular localization data of SnRK1.1 have not focused on the non-nuclear localization of this kinase (Supplementary Table S1). Only recently, it was shown by yeast two-hybrid experiments that the 18 members of the Arabidopis FCS-like zinc finger protein (FLZ) family interact promiscuously with SnRK1.1. Moreover, 10 of them

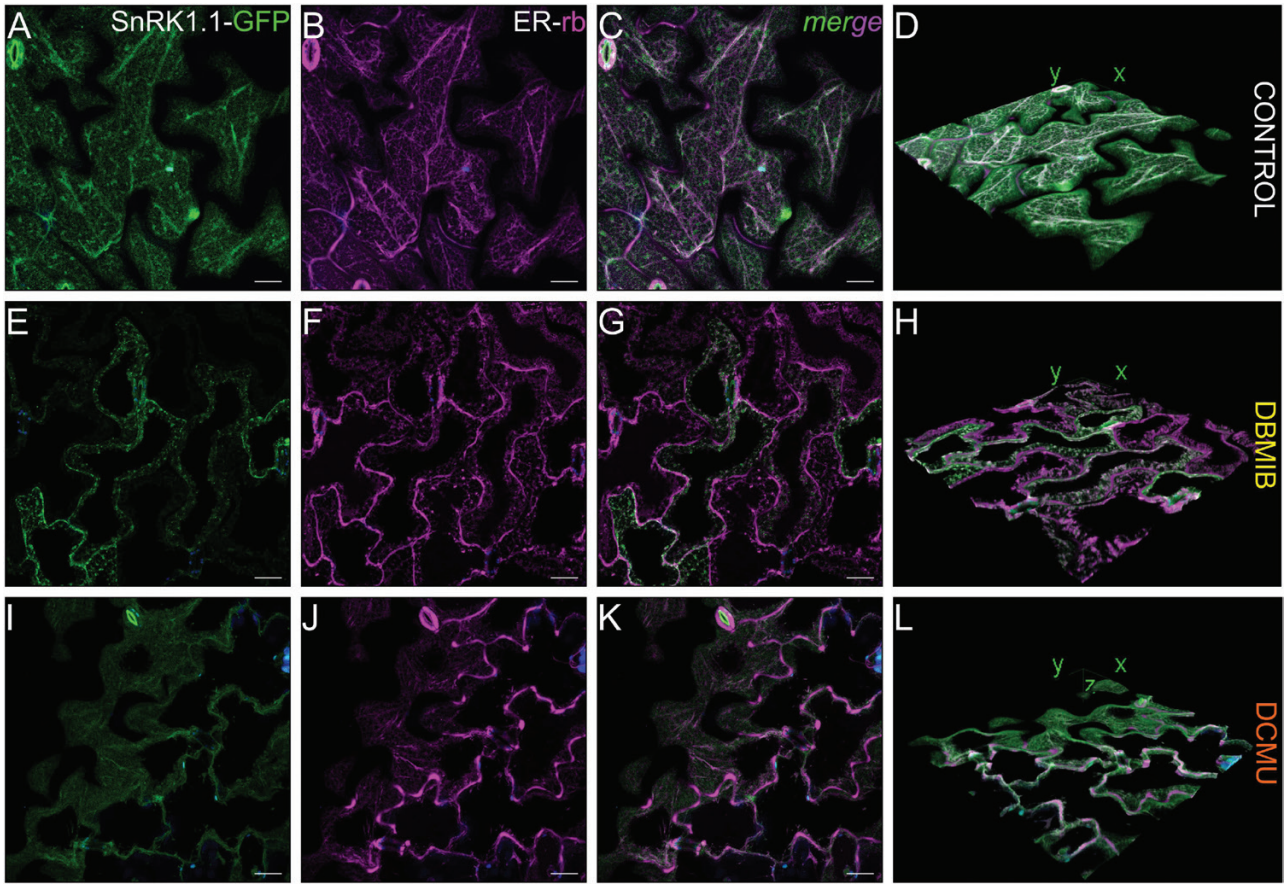

Fig. 6. Changes in SnRK1.1 and ER-rb marker distribution in response to perturbations in PETC. Study of leaf sections belonging to Arabidopsis stable transgenic lines simultaneously expressing SnRK1.1–GFP (green channel) and ER-rb (red channel) in response to DBMIB and DCMU treatments. Leaves were treated with the inhibitors of the PETC: 100 μM DBMIB (E–H) for 3 h and 50 μM DCMU (I–L) for 2h, and later analysed by LSCM. (A–C), (E–G), and (I–K) show the maximum intensity projection images of a 10 image *z*-stack series (Δz-axis ~0.49 μm) containing SnRK1.1 signal distribution, ER-rb signal, and both fluorescent signals merged for control and treated plants. (D, H, and L) 3D render reconstruction of the original *z*-stack images. The 3D reconstruction was generated using Fiji software. Scale bars: 20 μm.

were able to co-localize with ER-rb during bimolecular fluorescence complementation (BiFC) experiments with SnRK1.1 in onion epidermal cells (Jamsheer *et al*., 2018*a*, b). FLZ proteins have been interpreted to be scaffolds or adaptors to facilitate the assembly of the complexes containing SnRK1.1 (Jamsheer *et al*., 2018*b*). However, no functional meaning of the assembly of these complexes at the ER has been presented. In addition, these preliminary localization studies were conducted in heterologous systems and specialized tissues that lack functional chloroplasts.

In our current work, we use high-quality 3D imaging techniques and showed that SnRK1.1 is found in the nucleus as well as associated with the ER, mainly along ER strands and at the ER perinuclear ring. This was demonstrated by co-localization with two different ER markers, under physiological conditions in photosynthetic tissue. We used both *N. benthaminana* as well as stable expression in *A. thaliana* transgenic lines and the native regulatory sequence, which was crucial to avoid any artefacts affecting the imaging process. Considering the soluble character of SnRK1.1 itself, the lack of a predicted transmembrane domain in its sequence, and our localization results, we conclude that most probably the non-nuclear SnRK1.1 fraction is either bound to and/or interacting with proteins at the cytosolic face of the ER membrane. The strength of the association with the ER is also shown by the presence of SnRK1.1–GFP signal in the intracellular microsomal fraction. This fraction represents a subcellular pool of vesicles derived from the ER, providing extra evidence of the stability of the association with this organelle in both *N. benthamiana* and Arabidopsis. Moreover, co-localization experiments with ER-localized HMGR (Leivar *et al*., 2005; Ferrero *et al*., 2015; Rodríguez-Concepción and Boronat, 2015), which was conducted across a time series, demonstrated the stability of the association with the ER at least during a short time period. In these experiments, a highly dynamic behaviour characteristic of the HMGR and SnRK1.1 as ER-associated proteins was clearly observed.

HMGR is a well-known phosphorylation target of SnRK1.1 and catalyses the first committed step in the mevalonic acid biosynthetic pathway (Rodríguez-Concepción and Boronat, 2015). The SnRK1.1-mediated inactivation of HMGR is triggered by phosphorylation of a conserved serine residue located in the catalytic domain at the cytosolic face of the ER membrane-bound HMGR (Leivar *et al*., 2005; Antolín-Llovera *et al*., 2011; Ferrero *et al*., 2015; Robertlee *et al*., 2017). This co-localization therefore not only confirms ER association of

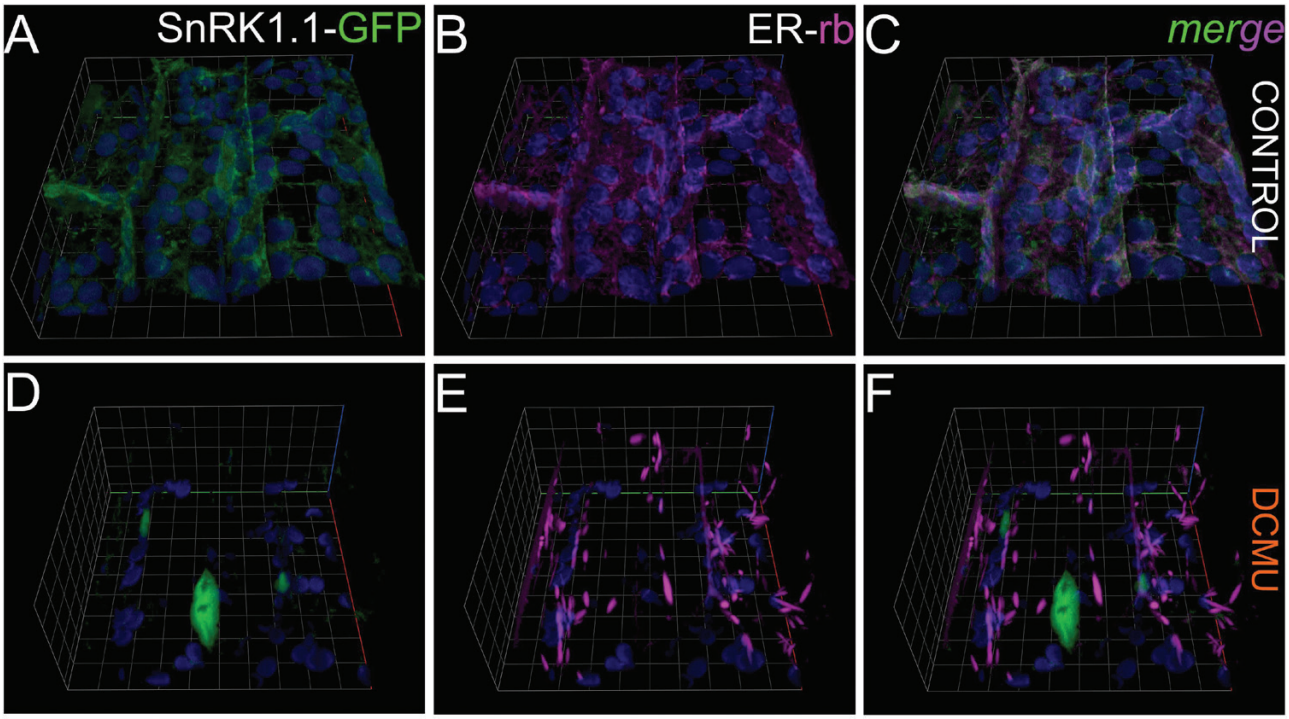

Fig. 7. Changes in SnRK1.1 distribution in response to perturbations at the PETC by DCMU. Panels present the 3D reconstruction of the *z*-stack image series of vascular tissue belonging to leaf sections of Arabidopsis stable transgenic lines simultaneously expressing SnRK1.1–GFP (green channel) and ER-rb (red channel). Treatments are similar to those in Fig. 6. The corresponding fluorescence channel or the image merging conditions are indicated at the top of the row. 3D reconstruction was generated by the Zen Zeiss 2012 (blue edition) software.

SnRK1.1 but also shows a potential direct functional output of this kinase at this organelle (Antolín-Llovera *et al.*, 2011).

In the frame of a model that places SnRK1 as a central integrator of stress and energy signals, SnRK1.1 has frequently been addressed as a gauge of central cellular energy status, integrating the functional status of the cellular powerhouses, chloroplasts and mitochondria (Hartl and Finkemeier 2012; Ng *et al.*, 2014; Kleine and Leister 2016). Following this hypothesis, it is tempting to hypothesize that the physical proximity between these organelles and the ER could facilitate the sensing of chloroplast and mitochondrial status by the ER-localized SnRK1.1 fraction (Prinz, 2014; Griffing *et al.*, 2017). For chloroplasts, different processes such as stromule formation, and exchange of metabolites including lipids and products of carotenoids have demonstrated the importance of the association between the ER and the plastid (Schattat *et al.*, 2011; Mehrshahi *et al.*, 2013; Griffing *et al.*, 2017; Barton *et al.*, 2018). One experimental example of such a structural and functional relationship between chloroplasts and the ER was the discovery of the transient changes in movement, behaviour, and aggregation status of ER-localized proteins in response to photostimulation of the chloroplast–ER interface (Griffing, 2011). To explore a link between SnRK1.1 localization and chloroplast status, we perturbed the photosynthetic electron flow with DCMU and DBMIB. Our aim was to mimic conditions of low- and high-energy status, respectively, and to reveal how these fluctuations might be sensed or perceived by the non-nuclear fraction of SnRK1.1. The observed dramatic changes in the distribution of the ER marker ER-rb, a protein in the ER, and in SnRK1.1 distribution in response to DBMIB, including the appearance of aggregates, was similar to the effect of chloroplast photostimulation (Griffing, 2011). On the other hand, a complete blockage of the electron flow via the plastoquinone pool by DCMU provoked variations in the intracellular distribution of SnRK1.1, with a strong relative increase in the nuclear fraction observed in vascular tissue. The DCMU treatment, leading to an overoxidized plastoquinone pool, affected the ER morphology in a different way, leading to spindle-shaped structures that resemble ER bodies. These structures have previously been associated with chloroplast perturbations, being induced specifically by the plastidial metabolite methylerythritol cyclodiphosphate (MEcPP), a precursor of plastidial isoprenoids (Wang *et al.*, 2017). These results revealed a link between fluctuations in plastid status and the ER proteome, and suggest a potential transduction of the plastidic energy status to ER-associated proteins including SnRK1.1. Moreover, the effect at the ER is not general but specific to the nature of the plastid imbalance.

The link between the plastid redox state and the function of the ER-associated SnRK1.1 can be orchestrated through redox-sensitive post-translational modification of this kinase (Wurzinger *et al.*, 2018). Based on the *in vitro* model presented by Wurzinger and collaborators, highly reductive plastids, such as the plastids following DBMIB treatments or when plants are exposed to high-light conditions, generate conditions that might favour the monomeric SnRK1.1 forms. Following the same rationale, under reductive conditions, SnRK1.1 is more active and phosphorylates targets such as bZIP63 (Wurzinger *et al.*, 2018). It would be interesting to evaluate the above-mentioned SnRK1.1 intracellular distribution changes

in response to plastid perturbations *in planta* using SnRK1.1 mutants insensitive to redox-based post-translational modifications. So far, among the SnRK1 subunits, a correlation between post-translational modification (myristoylation) and intracellular distribution has only been demonstrated for the β subunit 1 and 2 (SnRKβ1 and 2) (Pierre *et al.*, 2007). However, there is mounting evidence that the activity of SnRK1.1 is regulated by multiple post-translational modifications (Crozet *et al.*, 2014). In addition, the herein characterized dual localization of SnRK1.1 might be indicating how a compartmentalization–function relationship can be regulated via these modifications (Emanuelle *et al.*, 2016). Possible interactors that could play a role in this regulatory mechanism are for instance GRIK2/1 (Shen *et al.*, 2009), SnAK1/2 (Glab *et al.*, 2017), and ABI1/PP2C (Rodrigues *et al.*, 2013), which control the phosphorylation status of SnRK1.1.

The ER is a dynamic network formed by tubules and planar structures ideally arranged to act as a communication network throughout the cell connecting organelles such as mitochondria, chloroplasts, and the nucleus in an actin-dependent manner (Sparkes *et al.*, 2009*b*; Stefano *et al.*, 2014; Griffing *et al.*, 2017). This complex morphology turns the ER into an excellent candidate site as a hub for signal inputs from the whole cell and to convey this information to the nucleus to orchestrate an *ad hoc* response (Griffing *et al.*, 2017). The co-occurrence of other central stress signalling pathways with their key components (NAC013, NAC017, and Ire1) at the ER is part of the evidence supporting this concept (Koizumi *et al.*, 2001; De Clercq *et al.*, 2013; Ng *et al.*, 2013*b*). The finding of a dynamic ER-localized SnRK1.1–GFP fraction in close interaction with chloroplasts as shown by our localization studies underpins the idea of the ER as a hub of different signalling routes, including retrograde signals originating in the endosymbiotic organelles, and the potential involvement of SnRK1.1. The presence of SnRK1.1 at the ER, including in ER subdomains such as the perinuclear ring, might be essential for input and output of information of cellular energy status. The finding of RAPTOR1B, a component of the SnRK1-antagonist target of rapamycin (TOR) complex (Baena-González and Hanson, 2017), co-localizing with SnRK1.1 in the ER perinuclear ring, is highly interesting in this context (Nukarinen *et al.*, 2016). To probe the potential crosstalk between SnRK1 and TOR, integrated studies of the spatio-temporal distribution of the components of these complexes are challenges for the future.

Supplementary data

Supplementary data are available at *JXB* online.

Fig. S1. SnRK1.1 localization aspects obtained by bioinformatics tools.

Fig. S2. Nuclear localization of SnRK1.1 along the *z*-axis.

Fig. S3. SnRK1.1 localization in epidermal *N. benthamiana* cells using LSCM.

Fig. S4. Distribution of SnRK1.1 in vascular tissue of Arabidopsis stable transgenic lines expressing SnRK1.1.

Fig. S5. Spatial distribution of SnRK1.1 and ER-rb in *N. benthamiana* cells.

Fig. S6. Co-localization of SnRK1.1 with the ER resident protein 3-hydroxy-3-methylglutaryl coenzyme A reductase (HMGR).

Fig. S7. 3D reconstruction of the original *z*-stack images set of Fig. 4 generated using Fiji software.

Fig. S8. Loading controls and confirmation of the identity of the microsomal fraction.

Table S1. Summary of previous reports indicating SnRK1.1 localization.

Table S2. Co-localization by intensity correlation coefficient-based analysis in the cortical and nuclear zone.

Video S1. Spatial reconstruction of SnRK1.1–GFP and ER-rb signals by a fluorescent 3D model in *N. benthamiana*.

Video S2. Time frame sequence of the merged images of HMGR–GFP and SnRK1.1–mCherry corresponding to Supplementary Fig. S6.

Video S3. Spatial reconstruction of SnRK1.1 distribution with respect to ER by a fluorescent 3D model in Arabidopsis.

Acknowledgements

We would like wholeheartedly to thank to Anna Gustavsson, Josh Lynn, and Rodrigo Vena for their invaluable technical guidance in the whole imaging process of this work. Irene Martinez Carrasco [BICU Umeå University and the National Microscopy Infrastructure, NMI (VR-RFI 2016-00968)] is acknowledged for excellent technical assistance in experiments of DSU microscopy. Edouard Pesquet, Nicolás Bologna, Mikhail Shchepetilnikov, and Narciso Campos kindly provided H2b–RFP, ER-rb, and HMGR–GFP fluorescent markers, respectively. Estefania Mancini gave us an excellent input to understand the splicing behaviour of SnRK1.1, and we are in debt to Verena Kriechbaumer for her fruitful comments on the draft. Finally Fabiana Drincovich and Florencio Podestá are thanked for providing laboratory support. No conflict of interest is declared. This work was supported by grants from the Swedish Research Council, VR (ÅS), STINT and the Australian Research Council CE 140100008 (JW); and ICGEB (SMART Fellowship), FONCyT PICT2016-0093 and CONICET (NEB).

References

Allahverdiyeva Y, Battchikova N, Brosché M, *et al*. 2015*a*. Integration of photosynthesis, development and stress as an opportunity for plant biology. New Phytologist **208,** 647–655.

Allahverdiyeva Y, Suorsa M, Tikkanen M, Aro EM. 2015*b*. Photoprotection of photosystems in fluctuating light intensities. Journal of Experimental Botany **66,** 2427–2436.

Antolín-Llovera M, Leivar P, Arró M, Ferrer A, Boronat A, Campos N. 2011. Modulation of plant HMG-CoA reductase by protein phosphatase 2A: positive and negative control at a key node of metabolism. Plant Signaling & Behavior **6,** 1127–1131.

Araújo WL, Nunes-Nesi A, Fernie AR. 2014. On the role of plant mitochondrial metabolism and its impact on photosynthesis in both optimal and sub-optimal growth conditions. Photosynthesis Research **119,** 141–156.

Baena-González E, Hanson J. 2017. Shaping plant development through the SnRK1-TOR metabolic regulators. Current Opinion in Plant Biology **35,** 152–157.

Baena-González E, Rolland F, Thevelein JM, Sheen J. 2007. A central integrator of transcription networks in plant stress and energy signalling. Nature **448,** 938–942.

Barton KA, Wozny MR, Mathur N, Jaipargas E-A, Mathur J. 2018. Chloroplast behaviour and interactions with other organelles in *Arabidopsis thaliana* pavement cells. Journal of Cell Science **131,** jcs202275.

Bitrián M, Roodbarkelari F, Horváth M, Koncz C. 2011. BAC-recombineering for studying plant gene regulation: developmental control and cellular localization of SnRK1 kinase subunits. The Plant Journal **65,** 829–842.

Blanco NE, Guinea-Díaz M, Whelan J, Strand Å. 2014. Interaction between plastid and mitochondrial retrograde signalling pathways during changes to plastid redox status. Philosophical Transactions of the Royal Society B: Biological Sciences **369,** 20130231.

Bolte S, Cordelières FP. 2006. A guided tour into subcellular colocalization analysis in light microscopy. Journal of Microscopy **224,** 213–232.

Broeckx T, Hulsmans S, Rolland F. 2016. The plant energy sensor: evolutionary conservation and divergence of SnRK1 structure, regulation, and function. Journal of Experimental Botany **67,** 6215–6252.

Cecchini NM, Steffes K, Schläppi MR, Gifford AN, Greenberg JT. 2015. Arabidopsis AZI1 family proteins mediate signal mobilization for systemic defence priming. Nature Communications **6,** 7658.

Chakrabarty R, Banerjee R, Chung SM, Farman M, Citovsky V, Hogenhout SA, Tzfira T, Goodin M. 2007. PSITE vectors for stable integration or transient expression of autofluorescent protein fusions in plants: probing *Nicotiana benthamiana*–virus interactions. Molecular Plant-Microbe Interactions **20,** 740–750.

Chan KX, Phua SY, Crisp P, McQuinn R, Pogson BJ. 2016. Learning the languages of the chloroplast: retrograde signaling and beyond. Annual Review of Plant Biology **67,** 25–53.

Cho HY, Wen TN, Wang YT, Shih MC. 2016. Quantitative phosphoproteomics of protein kinase SnRK1 regulated protein phosphorylation in Arabidopsis under submergence. Journal of Experimental Botany **67,** 2745–2760.

Crawford T, Lehotai N, Strand Å. 2018. The role of retrograde signals during plant stress responses. Journal of Experimental Botany **69,** 2783–2795.

Crozet P, Margalha L, Confraria A, Rodrigues A, Martinho C, Adamo M, Elias CA, Baena-González E. 2014. Mechanisms of regulation of SNF1/AMPK/SnRK1 protein kinases. Frontiers in Plant Science **5,** 190.

De Clercq I, Vermeirssen V, Van Aken O, *et al*. 2013. The membrane-bound NAC transcription factor ANAC013 functions in mitochondrial retrograde regulation of the oxidative stress response in Arabidopsis. The Plant Cell **25,** 3472–3490.

de Felippes FF, Weigel D. 2010. Transient assays for the analysis of miRNA processing and function. Methods in Molecular Biology **592,** 255–264.

Emanuelle S, Doblin MS, Stapleton DI, Bacic A, Gooley PR. 2016. Molecular insights into the enigmatic metabolic regulator, SnRK1. Trends in Plant Science **21,** 341–353.

Ferrero S, Grados-Torrez RE, Leivar P, Antolín-Llovera M, López-Iglesias C, Cortadellas N, Ferrer JC, Campos N. 2015. Proliferation and morphogenesis of the endoplasmic reticulum driven by the membrane domain of 3-hydroxy-3-methylglutaryl coenzyme A reductase in plant cells. Plant Physiology **168,** 899–914.

Glab N, Oury C, Guérinier T, Domenichini S, Crozet P, Thomas M, Vidal J, Hodges M. 2017. The impact of *Arabidopsis thaliana* SNF1-related-kinase 1 (SnRK1)-activating kinase 1 (SnAK1) and SnAK2 on SnRK1 phosphorylation status: characterization of a SnAK double mutant. The Plant Journal **89,** 1031–1041.

Griffing LR. 2011. Laser stimulation of the chloroplast/endoplasmic reticulum nexus in tobacco transiently produces protein aggregates (boluses) within the endoplasmic reticulum and stimulates local ER remodeling. Molecular Plant **4,** 886–895.

Griffing LR, Lin C, Perico C, White RR, Sparkes I. 2017. Plant ER geometry and dynamics: biophysical and cytoskeletal control during growth and biotic response. Protoplasma **254,** 43–56.

Hardie DG, Schaffer BE, Brunet A. 2016. AMPK: an energy-sensing pathway with multiple inputs and outputs. Trends in Cell Biology **26,** 190–201.

Hartl M, Finkemeier I. 2012. Plant mitochondrial retrograde signaling: post-translational modifications enter the stage. Frontiers in Plant Science **3,** 253.

Hawes C, Kiviniemi P, Kriechbaumer V. 2015. The endoplasmic reticulum: a dynamic and well-connected organelle. Journal of Integrative Plant Biology **57,** 50–62.

Hooper CM, Castleden IR, Tanz SK, Aryamanesh N, Millar AH. 2017. SUBA4: the interactive data analysis centre for Arabidopsis subcellular protein locations. Nucleic Acids Research **45,** D1064–D1074.

Jamsheer K M, Sharma M, Singh D, Mannully CT, Jindal S, Shukla BN, Laxmi A. 2018*a*. FCS-like zinc finger 6 and 10 repress SnRK1 signalling in Arabidopsis. The Plant Journal **94,** 232–245.

Jamsheer K M, Shukla BN, Jindal S, Gopan N, Mannully CT, Laxmi A. 2018*b*. The FCS-like zinc finger scaffold of the kinase SnRK1 is formed by the coordinated actions of the FLZ domain and intrinsically disordered regions. Journal of Biological Chemistry **293,** 13134–13150.

Kindgren P, Kremnev D, Blanco NE, de Dios Barajas López J, Fernández AP, Tellgren-Roth C, Kleine T, Small I, Strand A. 2012. The plastid redox insensitive 2 mutant of Arabidopsis is impaired in PEP activity and high light-dependent plastid redox signalling to the nucleus. The Plant Journal **70,** 279–291.

Kleine T, Leister D. 2016. Retrograde signaling: organelles go networking. Biochimica et Biophysica Acta **1857,** 1313–1325.

Koizumi N, Martinez IM, Kimata Y, Kohno K, Sano H, Chrispeels MJ. 2001. Molecular characterization of two Arabidopsis Ire1 homologs, endoplasmic reticulum-located transmembrane protein kinases. Plant Physiology **127,** 949–962.

Kriechbaumer V. 2016. ER microsome preparation and subsequent IAA quantification in maize coleoptile and primary root tissue. Bio-Protocol **6,** e1085.

Kriechbaumer V, Seo H, Park WJ, Hawes C. 2015. Endoplasmic reticulum localization and activity of maize auxin biosynthetic enzymes. Journal of Experimental Botany **66,** 6009–6020.

Leivar P, González VM, Castel S, Trelease RN, López-Iglesias C, Arró M, Boronat A, Campos N, Ferrer A, Fernàndez-Busquets X. 2005. Subcellular localization of Arabidopsis 3-hydroxy-3-methylglutaryl-coenzyme A reductase. Plant Physiology **137,** 57–69.

López-Paz C, Vilela B, Riera M, Pagès M, Lumbreras V. 2009. Maize AKINbetagamma dimerizes through the KIS/CBM domain and assembles into SnRK1 complexes. FEBS Letters **583,** 1887–1894.

Mair A, Pedrotti L, Wurzinger B, *et al*. 2015. SnRK1-triggered switch of bZIP63 dimerization mediates the low-energy response in plants. eLife **4,** e05828.

Mancini E, Sanchez SE, Romanowski A, Schlaen RG, Sanchez-Lamas M, Cerdán PD, Yanovsky MJ. 2016. Acute effects of light on alternative splicing in light-grown plants. Photochemistry and Photobiology **92,** 126–133.

Mao YS, Zhang B, Spector DL. 2011. Biogenesis and function of nuclear bodies. Trends in Genetics **27,** 295–306.

Mehrshahi P, Stefano G, Andaloro JM, Brandizzi F, Froehlich JE, DellaPenna D. 2013. Transorganellar complementation redefines the biochemical continuity of endoplasmic reticulum and chloroplasts. Proceedings of the National Academy of Sciences, USA **110,** 12126–12131.

Nelson BK, Cai X, Nebenführ A. 2007. A multicolored set of in vivo organelle markers for co-localization studies in Arabidopsis and other plants. The Plant Journal **51,** 1126–1136.

Ng S, De Clercq I, Van Aken O, Law SR, Ivanova A, Willems P, Giraud E, Van Breusegem F, Whelan J. 2014. Anterograde and retrograde regulation of nuclear genes encoding mitochondrial proteins during growth, development, and stress. Molecular Plant **7,** 1075–1093.

Ng S, Giraud E, Duncan O, *et al*. 2013*a*. Cyclin-dependent kinase E1 (CDKE1) provides a cellular switch in plants between growth and stress responses. Journal of Biological Chemistry **288,** 3449–3459.

Ng S, Ivanova A, Duncan O, *et al*. 2013*b*. A membrane-bound NAC transcription factor, ANAC017, mediates mitochondrial retrograde signaling in Arabidopsis. The Plant Cell **25,** 3450–3471.

Nietzsche M, Landgraf R, Tohge T, and Börnke F. 2016. A protein–protein interaction network linking the energy-sensor kinase SnRK1 to multiple signaling pathways in *Arabidopsis thaliana*. Current Plant Biology **5,** 36–44.

Nietzsche M, Schießl I, Börnke F. 2014. The complex becomes more complex: protein–protein interactions of SnRK1 with DUF581 family proteins provide a framework for cell- and stimulus type-specific SnRK1 signaling in plants. Frontiers in Plant Science **5,** 54.

Nukarinen E, Nägele T, Pedrotti L, *et al*. 2016. Quantitative phosphoproteomics reveals the role of the AMPK plant ortholog SnRK1 as a metabolic master regulator under energy deprivation. Scientific Reports **6,** 31697.

O'Brien M, Kaplan-Levy RN, Quon T, Sappl PG, Smyth DR. 2015. PETAL LOSS, a trihelix transcription factor that represses growth in *Arabidopsis thaliana*, binds the energy-sensing SnRK1 kinase AKIN10. Journal of Experimental Botany **66,** 2475–2485.

Pierre M, Traverso JA, Boisson B, Domenichini S, Bouchez D, Giglione C, Meinnel T. 2007. N-myristoylation regulates the SnRK1 pathway in Arabidopsis. The Plant Cell **19,** 2804–2821.

Prinz WA. 2014. Bridging the gap: membrane contact sites in signaling, metabolism, and organelle dynamics. Journal of Cell Biology **205,** 759–769.

Robertlee J, Kobayashi K, Suzuki M, Muranaka T. 2017. AKIN10, a representative Arabidopsis SNF1-related protein kinase 1 (SnRK1), phosphorylates and downregulates plant HMG-CoA reductase. FEBS Letters **591,** 1159–1166.

Rochaix JD. 2011. Regulation of photosynthetic electron transport. Biochimica et Biophysica Acta **1807,** 375–383.

Rodrigues A, Adamo M, Crozet P, *et al*. 2013. ABI1 and PP2CA phosphatases are negative regulators of Snf1-related protein kinase1 signaling in Arabidopsis. The Plant Cell **25,** 3871–3884.

Rodríguez-Concepción M, Boronat A. 2015. Breaking new ground in the regulation of the early steps of plant isoprenoid biosynthesis. Current Opinion in Plant Biology **25,** 17–22.

Schattat M, Barton K, Baudisch B, Klösgen RB, Mathur J. 2011. Plastid stromule branching coincides with contiguous endoplasmic reticulum dynamics. Plant Physiology **155,** 1667–1677.

Shen W, Reyes MI, Hanley-Bowdoin L. 2009. Arabidopsis protein kinases GRIK1 and GRIK2 specifically activate SnRK1 by phosphorylating its activation loop. Plant Physiology **150,** 996–1005.

Sparkes IA, Frigerio L, Tolley N, Hawes C. 2009*a*. The plant endoplasmic reticulum: a cell-wide web. The Biochemical Journal **423,** 145–155.

Sparkes I, Runions J, Hawes C, Griffing L. 2009*b*. Movement and remodeling of the endoplasmic reticulum in nondividing cells of tobacco leaves. The Plant Cell **21,** 3937–3949.

Sparkes IA, Runions J, Kearns A, Hawes C. 2006. Rapid, transient expression of fluorescent fusion proteins in tobacco plants and generation of stably transformed plants. Nature Protocols **1,** 2019–2025.

Sperschneider J, Catanzariti AM, DeBoer K, Petre B, Gardiner DM, Singh KB, Dodds PN, Taylor JM. 2017. LOCALIZER: subcellular localization prediction of both plant and effector proteins in the plant cell. Scientific Reports **7,** 44598.

Stefano G, Hawes C, Brandizzi F. 2014. ER—the key to the highway. Current Opinion in Plant Biology **22,** 30–38.

Tsai AY, Gazzarrini S. 2012. AKIN10 and FUSCA3 interact to control lateral organ development and phase transitions in Arabidopsis. The Plant Journal **69,** 809–821.

Wang JZ, Li B, Xiao Y, *et al*. 2017. Initiation of ER body formation and indole glucosinolate metabolism by the plastidial retrograde signaling metabolite, MEcPP. Molecular Plant **10,** 1400–1416.

Weigel A, Schild D, Zeug A. 2009. Resolution in the ApoTome and the confocal laser scanning microscope: comparison. Journal of Biomedical Optics **14,** 014022.

Williams SP, Rangarajan P, Donahue JL, Hess JE, Gillaspy GE. 2014. Regulation of sucrose non-fermenting related kinase 1 genes in *Arabidopsis thaliana*. Frontiers in Plant Science **5,** 324.

Winter D, Vinegar B, Nahal H, Ammar R, Wilson GV, Provart NJ. 2007. An 'Electronic Fluorescent Pictograph' browser for exploring and analyzing large-scale biological data sets. PLoS One **2,** e718.

Wurzinger B, Nukarinen E, Nägele T, Weckwerth W, Teige M. 2018. The SnRK1 kinase as central mediator of energy signaling between different organelles. Plant Physiology **176,** 1085–1094.

Yoshida K, Watanabe CK, Terashima I, Noguchi K. 2011. Physiological impact of mitochondrial alternative oxidase on photosynthesis and growth in *Arabidopsis thaliana*. Plant, Cell & Environment **34,** 1890–1899.